

Theoretical Study of the Hydrolysis of Pentameric Aluminum Complexes

Jaakko Saukkoriipi[†] and Kari Laasonen*

Department of Chemistry, University of Oulu, P.O. Box 3000, Oulu FI-90014, Finland

Received December 14, 2009

Abstract: Static quantum chemical calculations and Car–Parrinello molecular dynamics (CPMD) simulations were used to investigate the structural characteristics and the stability of pentameric aluminum clusters in both gas phase and aquatic environments. The accuracy of several generalized gradient approximation (GGA) and hybrid exchange-correlation functionals were tested with and without empirical van der Waals corrections to ensure the accuracy of the selected methods. Conformational analysis was performed for experimentally detected (electrospray ionization mass spectrometry, ESI MS) structural isomers of cationic $[Al_5O_6H_2Cl_4]^+$, $[Al_5O_7H_4Cl_4]^+$, $[Al_5O_8H_6Cl_4]^+$, and $[Al_5O_9H_8Cl_4]^+$ complexes. Conductor-like screening model (COSMO) was used to investigate the stability of the gas phase optimized structures in aquatic environments. Four of the main pentameric aluminum complexes were then selected for the CPMD investigation. The effect of the long-range empirical vdW corrections (-D) was also tested employing two identical simulations, with and without the corrections. During these simulations, several spontaneous associative hydration reactions were detected. The open and highly symmetric hexagonal prism-like structures were found to be dominating geometries in liquid conditions. Overall, CPMD calculations produced distinctly different geometries for the pentameric molecules than for the static calculations.

1. Introduction

The speciation of aluminum compounds in aquatic environments has been widely studied both experimentally and theoretically during the past few decades. Experimental methods, such as potentiometric titration,^{1,2} ²⁷Al nuclear magnetic resonance (NMR) spectroscopy,^{3–10} X-ray crystallography,^{11,12} and electrospray ionization mass spectrometry (ESI MS)^{13–17} have been used to reveal the hydrolysis of aluminum salts during coagulation in aquatic solutions. At the same time, several computational studies have addressed the structures and energetics of different sized aluminum compounds and ions in gas phase and in liquid environments.^{18–29} As a result of these investigations, a wide variety

of different aluminum species have been detected from small monomeric to large polynuclear aluminum complexes. However, there are still a number of unknown factors concerning the exact nature and composition of the hydrolysis products of aluminum salts in aqueous environments. One of the most interesting factors is the role of small oligomeric species, like pentameric aluminum complexes in the aforementioned hydrolysis processes.

The first real evidence of the existence of pentameric aluminum complexes in aquatic solutions was detected in the high-field ¹H and ²⁷Al NMR studies of Akitt et al.³⁰ They postulated that, at higher aluminum concentrations (>0.02 mol dm⁻³) and at intermediate levels of hydrolysis, an oligomeric mixture of $[Al(OH)_{2.5}]^{0.5+}$ is formed, which can then be composed of pentameric aluminum complexes, like $[Al_5(OH)_{12}]^{3+}$ and $[Al_5(OH)_{13}]^{2+}$.³⁰ However, the results of Akitt et al. indicated that these oligomeric aluminum species were only intermediate forms in polymerization from monomers to the tridecameric “Keggin” cation $[AlO_4Al_{12}-(OH)_{24}(H_2O)_{12}]^{7+}$, especially in low aluminum concentrations

* Corresponding author phone: +358 8 553 1640; fax: +358 8 553 1603; e-mail: kari.laasonen@oulu.fi.

[†] Present address: Finnish Environment Institute (SYKE), Freshwater Centre, River Basin Management, The Oulu Office, P.O. Box 413, FI-90014, University of Oulu, Finland. E-mail: jaakko.saukkoriipi@ymparisto.fi.

(<0.02 mol dm⁻³).^{30,31} Two decades later, Sarpola et al. investigated the hydrolysis products of aluminum in the aquatic environments using the ESI MS method and detected around 20 different cationic pentameric aluminum complexes mainly at 10–100 mM aluminum concentrations in acidic solutions (pH < 4.7).^{13–15} They also postulated that pentameric structures seemed to be surprisingly stable in aquatic environments.³²

Recently, Zhao et al. studied the effect of pH to the hydrolysis of aluminum salts using the ESI MS method and discovered only one pentameric aluminum complex ($[Al_5O_7]^{+}$), which was present mainly at the pH range of 4.0–5.0.¹⁷ Zhao et al. postulated also two mechanisms for the coagulation of aluminum salts, the “core-link” and “cage-like” models. In the “cage-like” model, there are only monomeric, dimeric, and tridecameric polycations and larger polynuclear aluminum species in the aquatic solutions.¹⁷ However, the “core-links” model gives a distribution of continuously changed aluminum compounds from monomeric species to smaller oligomeric aluminum complexes, etc.¹⁷ Zhao et al. claimed that pentameric aluminum complexes can either fragment to tetrameric aluminum compounds by loosing an aluminum atom or aggregate by self-assembly to form larger aluminum complexes (Al_{10}) in aquatic environments.¹⁷ They also postulated that small oligomeric aluminum compounds (Al_3 – Al_5) are dominating in the pH range of 4.6–4.8 at very low aluminum concentrations (1.5×10^{-4} mol dm⁻³).

Das et al. combined quantum chemical density functional calculations with anion photoelectron and mass spectroscopy. They investigated the structural characteristics of neutral and anionic Al_5O_4 clusters.^{33,34} Highly symmetric planar geometry was detected to be the ground state structure for the anionic aluminum oxide cluster $Al_5O_4^-$. In addition, a neutral Al_5O_4 cluster was observed to have very large electron affinity, equivalent with the affinity of the chlorine ion.³⁴ The results of the photoelectron spectroscopy revealed the high reactivity of the anionic cluster toward an aqua ligand. Reactivity was then confirmed in the static quantum chemical density functional calculations.³³ Although pentameric aluminum clusters have been studied both experimentally and theoretically, there are still a number of uncertainties concerning their stability and structural characteristics in the hydrolysis processes.

In this investigation, we have studied the characteristics of cationic pentameric aluminum complexes in aquatic environments using static quantum chemical methods and Car–Parrinello molecular dynamics (CPMD) simulations. Pentameric complexes were taken directly from the ESI MS results of Sarpola et al.^{13–15,32} It should be noted that most of the time, especially when the fragmentation series of aqua ligands or isotopic patterns are lacking in the spectra, ESI MS gives only the sum mass of the complex.¹⁴ Hence, quantum chemical conformational analysis was performed to obtain the lowest energy conformations of the chosen pentameric species prior to the ab initio molecular dynamics (AIMD) simulations. The main goal of this study was to reveal the stability of the pentameric aluminum complexes in aquatic environments and, in addition, to elucidate their

role in the aforementioned hydrolysis processes. The secondary objective was to investigate the applicability of the empirical van der Waals corrections to both static calculations and CPMD simulations.

2. Computational Details

2.1. Static, Gas Phase Studies. We investigated the structures of aluminum complexes with the molecular formulas of $[Al_5O_6H_2Cl_4]^+$, $[Al_5O_7H_4Cl_4]^+$, $[Al_5O_8H_6Cl_4]^+$, and $[Al_5O_9H_8Cl_4]^+$. We note that these were the main pentameric aluminum species detected in the ESI MS studies of Sarpola et al.^{13–15,32} Geometry optimizations were carried out without symmetry constraints. The structural optimization of the clusters were performed using density functional theory (DFT) with the Perdew–Burke–Ernzerhof (PBE) functional³⁵ and polarized valence triple ζ (TZVP) basis set.³⁶ Calculations were performed using the Turbomole 6.0 program suite.³⁷ Resolution-of-the-identity (RI) approximation was used to accelerate the calculations.³⁸

The choice of PBE density functional was justified with a test of four trimeric, four tetrameric, and four pentameric aluminum (chloro)hydroxide complexes, which were then optimized in the gas phase with different methods (Becke88 exchange and Lee–Yang–Parr correlation functional (BLYP), Becke’s three parameter hybrid functional (B3LYP)) with the TZVP basis set. The accuracy and the effect of empirical van der Waals corrections (-D) were also tested here (PBE and B3LYP).³⁹ For the usage of these corrections, three sets of parameters must be defined, density functional dependent global scaling factor s_6 , dispersion coefficients C_6 ([Jnm⁶ mol⁻¹]), and van der Waals radii R_0 (Å) for the elements.⁴⁰ Scaling factor s_6 for PBE was 0.75 and 1.05 for B3LYP. The C_6 and R_0 parameters for aluminum were 10.79 and 1.639, for oxygen 0.70 and 1.342, for hydrogen 0.14 and 1.001, and for chlorine 5.07 and 1.639. The total energy is then given by equation

$$E_{DFT-D} = E_{DFT} + \left(-s_6 \sum_{i=1}^{N_{at}-1} \sum_{j=i+1}^{N_{at}} \frac{C_6^{ij}}{R_{ij}^6} f_{\text{dmp}}(R_{ij}) \right) \quad (1)$$

N_{at} denotes the number of atoms in a system, C_6^{ij} is the dispersion coefficient for atom pair ij that can be written as geometric mean ($(C_6^i C_6^j)^{1/2}$). We note that the selected trimeric and tetrameric complexes came from the previous studies of the author.⁴¹ Second-order Møller–Plesset perturbation theory (MP2) with the frozen core approximation and quadruple ζ valence with double polarization (QZVPP) was chosen for the reference method, see Table 1.^{42–44}

The justification of the frozen core approximation is that the inner-shell electrons of an atom are less sensitive to their environment than the valence electrons. Thus, the error introduced by freezing the core orbitals is nearly constant for molecules containing the same types of atoms. The accuracy of this approximation was also tested by fully optimizing the selected aluminum structures in the MP2/QZVPP level of theory with and without frozen core approximation. Approximation clearly accelerated the optimization procedure but had only a mild affect to the relative

Table 1. Comparison of the Gas Phase Energy Differences [kJ mol⁻¹] of Aluminum Chlorohydrates

cluster	PBE	BLYP	B3LYP ^a	PBE-D	B3LYP-D ^a	MP2/QZVPP
[Al ₃ O ₇ H ₉ Cl ₃] ⁺ _1	19.0	25.3	25.5	26.5	35.7	23.3
[Al ₃ O ₇ H ₉ Cl ₃] ⁺ _2	32.9	27.0	28.6	32.9	28.5	32.7
[Al ₃ O ₇ H ₉ Cl ₃] ⁺ _3	3.1	1.5	2.0	3.3	1.9	4.2
[Al ₃ O ₇ H ₉ Cl ₃] ⁺ _4	0	0	0	0	0	0
[Al ₄ O ₈ H ₉ Cl ₄] ⁺ _1	25.7	22.5	23.5	27.8	25.9	24.8
[Al ₄ O ₈ H ₉ Cl ₄] ⁺ _2	57.4	47.5	51.2	49.8	40.2	52.3
[Al ₄ O ₈ H ₉ Cl ₄] ⁺ _3	35.0	24.1	32.7	39.4	33.7	45.5
[Al ₄ O ₈ H ₉ Cl ₄] ⁺ _4	0	0	0	0	0	0
[Al ₅ O ₇ H ₄ Cl ₄] ⁺ _1	56.9	44.8	50.0	45.9	34.4	49.3
[Al ₅ O ₇ H ₄ Cl ₄] ⁺ _2	40.4	28.3	31.9	35.6	25.3	38.2
[Al ₅ O ₇ H ₄ Cl ₄] ⁺ _3	49.8	53.0	55.9	47.4	53.0	49.9
[Al ₅ O ₇ H ₄ Cl ₄] ⁺ _4	0	0	0	0	0	0
average ^b	2.7	4.7	3.1	2.0	6.2	
standard deviation ^b	3.5	6.0	3.8	1.9	6.0	

^a Without resolution-of-the-identity (RI) approximation. ^b Calculated from the absolute values of $|\Delta E_{\text{MP2}} - \Delta E_{\text{DFTI}}|$.

energy differences between chosen aluminum conformations (0.1–5.9 kJ mol⁻¹). The accuracy of the chosen theory was also tested against the second-order approximate coupled-cluster (CC2/QZVPP) method. This was done optimizing five dimeric ([Al₂O₆H₉Cl₂]⁺)⁴¹, and eight trimeric (four [Al₃O₇H₈Cl₃]⁺ and four [Al₃O₇H₈SO₄]⁺)^{16,41} aluminum conformations with the CC2 level of theory without frozen core approximation and comparing the relative energy differences to the MP2 results. The linear regression analysis of the relative energy differences were very close to linear dependency; the goodness of fit (R^2) was 0.9996. The results of these tests confirmed clearly that the accuracy of the MP2/QZVPP/frozen core approximation level of theory is sufficient for the reference method.

The comparison of the accuracy of the chosen methods (Table 1) was performed by subtracting the relative energy differences of trimeric, tetrameric, and pentameric aluminum complexes calculated with different density functional or hybrid methods from the corresponding relative energy differences of the reference method. This was followed by taking the absolute values of the extractions. Then, the averages and standard deviations were calculated of the absolute values; see Table 1. Note that the ground state energies were also included ($n = 12$). The results showed that the PBE functional gives slightly more consistent results compared to the BLYP density functional^{45,46} and B3LYP hybrid functional^{45–48} with lower mean value and standard deviation. The van der Waals-corrected functionals yielded the following results; the PBE-D had the lowest mean value and standard deviation of the test, whereas B3LYP-D had the highest. The results indicated clearly that the empirical corrections can either enhance the accuracy of the functional (PBE) or worsen it (B3LYP). Due to this test, the PBE density functional with triple ζ basis set was chosen for the preliminary optimizations and the PBE with empirical van der Waals corrections was chosen for the verification.

During the test, we examined also the double-hybrid functional B2PLYP-D with long-range empirical dispersion corrections.^{45–47,49,50} We tested its accuracy using the second-order approximate coupled cluster (CC2/QZVPP) as the reference, although B2PLYP-D can only be used for single point calculations in Turbomole. It is a new type of hybrid density functional with global parameters of α_x for describing the mixture of Hartree–Fock (HF) and generalized

gradient approximation (GGA) exchange and \mathbf{c} for describing the perturbative second-order correlation part (PT2) and GGA correlation.^{49,50} The relative energy differences of different dimeric and trimeric aluminum chlorohydrate conformations calculated with the B2PLYP-D/TZVP level of theory were then subtracted from CC2/QZVPP results taking the absolute values from the differences. The high standard deviation (15.6) and rather high mean value (8.2) of the differences indicate that the new double-hybrid density functional (DHDF) is not the best choice for describing the chemical nature and relative energy differences of aluminum (chloro)hydroxide complexes. The new DHDF was also tested for tetrameric and pentameric aluminum chlorohydrates using MP2/QZVPP with frozen core approximation as a reference. In the case of small oligomeric aluminum complexes, not only the standard deviations and mean values increased but also the functional failed to describe the trends in energy differences of different conformations compared to the results of any other density functional or reference method. These observations show clearly that the B2PLYP-D is not a suitable method for cationic aluminum (chloro)hydroxide calculations and, hence, was not used in further investigations in this study.

2.2. Static, Liquid Phase Calculations. The stability of gas phase optimized structures in aqueous environments was investigated using conductor-like screening model (COSMO) with triple ζ valence with double polarization.^{36,51,52} COSMO is a solvation model, where the solute forms a cavity within the dielectric continuum of the permittivity ϵ that represents the solvent.³⁷ In this study, water ($\epsilon = 78.39$) was chosen for the solvent. Most of the parameters employed were the default parameters of COSMO, e.g., optimized van der Waals radii for O, H, and Cl atoms existed in the code. The radius for chlorine was 2.05 Å, for oxygen 1.72 Å, and for hydrogen 1.30 Å, and the scaling factor was approximately 1.89. However, the van der Waals radius of the aluminum ion (R_{Al}) had to be defined computationally. It was determined as follows. The literature value for the Gibbs free energy of hydration of Al³⁺ ion is −4619 kJ mol⁻¹.⁵³ Burgess introduced Gibbs free energies of the hydration for the cations relative to the estimated free energy of the hydration of a proton (−1090.7 kJ mol⁻¹).⁵³ Tissandier et al. corrected and updated the value of the absolute Gibbs free energy of the hydration of the proton by less than 14 kJ

mol^{-1} ($-1104.5 \text{ kJ mol}^{-1}$) in their Cluster-Pair-Based approximation studies.⁵⁴ The value of the Gibbs free energy of aluminum ion was then corrected according to the correction of Tissandier et al.⁵⁴

The optimized COSMO radius for aluminum ion was calculated using eq 2, where $\Delta E_{\text{COSMO}}(\text{Al}^{3+}, R_{\text{Al}})$ is the COSMO-corrected total energy of Al^{3+} ion and $\Delta E_{\text{vacuum}}(\text{Al}^{3+})$ is the total energy of Al^{3+} ion in gas phase. The optimized van der Waals radius for aluminum ion was then specified to 1.3287 Å. Coskuner et al. postulated a similar van der Waals radius for aluminum (1.33) in their coordination studies of Al-EDTA in aqueous solutions.⁵⁵

$$\Delta E_{\text{Solv}}(\text{Al}^{3+}) = \Delta E_{\text{COSMO}}(\text{Al}^{3+}, R_{\text{Al}}) - \Delta E_{\text{vacuum}}(\text{Al}^{3+}) \quad (2)$$

During this research, all COSMO calculations were made as single point calculations. The choice was made to compare the solvation energy differences of gas phase optimized conformations without altering the gas phase structures. The choice can be rationalized with the fact that the measuring process in the ESI MS method takes place in vacuum conditions.^{13–16} However, the choice of single point COSMO calculations has been tested in reference to the full COSMO optimization calculations in our previous computational studies.^{16,41} More detailed description of the tests can be found in refs 16 and 41.

2.3. Car–Parrinello Molecular Dynamics Simulations. Pentameric aluminum complexes were also studied in a liquid environment using ab initio molecular dynamics (AIMD)-simulations. The selected pentameric species were $[\text{Al}_5\text{O}_6\text{H}_2\text{Cl}_4]^+$ ($m/z = 373$) and $[\text{Al}_5\text{O}_7\text{H}_4\text{Cl}_4]^+$ ($m/z = 391$). The initial molecular formulas for the pentameric aluminum clusters came from the ESI MS studies of Sarpola et al.^{13–16,32} The minimum energy structures for chosen oligomeric aluminum clusters were then deduced in gas phase in the static part of this study. Three different conformations including the gas phase minima of the cationic $[\text{Al}_5\text{O}_6\text{H}_2\text{Cl}_4]^+$ complex were taken and placed into a 17.0 Å cubic shell and solvated by 141 explicit water molecules, producing a density of 1.04 g cm⁻³. In addition, the gas phase minima of the cationic $[\text{Al}_5\text{O}_7\text{H}_4\text{Cl}_4]^+$ cluster was solvated by 169 water molecules in a cubic shell of 18.0 Å sides, producing a density of 1.04 g cm⁻³. Note that densities were calculated for a deuterated system. The initial guess of the water molecule positions was based on the simple point charge (SPC) water model.^{56,57}

We used 24 Ry cutoffs for the plane wave expansion and periodic boundary conditions. Simulations were performed in the canonical ensembles (NVT) using a Car–Parrinello molecular dynamics approach (CPMD).⁵⁸ The temperature of the simulations was scaled to 350 K using a chain of Nose–Hoover thermostats^{59–62} with characteristic frequency of 2500 cm⁻¹, which was fixed high enough to ensure that the OH moieties were thermostatted properly and to have better control of fictitious kinetic energy. The core electrons were described using Vanderbilt ultra soft pseudopotentials^{63–65} for all atoms in a system. The time step for electrons and ions in these simulations was 6 atomic units (0.145 fs), which was possible using deuterium instead of hydrogen in the simulations. The following atomic masses for the nuclei were

used 2.0 amu for hydrogen, 16.0 amu for oxygen, 27.0 amu for aluminum, and 35.4 amu for chlorine atoms. Fictitious electron mass (μ) was 650 atomic units, and the total charge of the system was +1. The equations of motion were solved using velocity Verlet algorithm.

PBE density functional³⁵ was used throughout the simulations. It was selected for the investigations due to the proven accuracy in describing the structural characteristics and stability of the aluminum chlorohydroxides in aquatic environments.⁶⁶ The effect of empirical van der Waals corrections was also tested during this research. Simulations were performed with and without van der Waals corrections. Corrections were employed using the ALL GRIMME approach, where long-range dispersion forces are considered by explicitly including damped pairwise interatomic potentials of $C_6^{ij}R_{ij}^{-6}$ form in the total energy.^{39,40} The average simulation times were from 30 to 45 ps throughout this investigation.

3. Results and Discussion

3.1. Static Calculations. In this part, we will focus on the structural characteristic of the cationic pentameric aluminum complexes, $[\text{Al}_5\text{O}_6\text{H}_2\text{Cl}_4]^+$, $[\text{Al}_5\text{O}_7\text{H}_4\text{Cl}_4]^+$, $[\text{Al}_5\text{O}_8\text{H}_6\text{Cl}_4]^+$, and $[\text{Al}_5\text{O}_9\text{H}_8\text{Cl}_4]^+$. We will discuss the conformational isomers of the aluminum clusters above and compare the characteristics of the most interesting low energy conformations. In total, we have investigated hundreds of planar and nonplanar configurations of the oligomeric aluminum species for the geometry optimizations. The structures were optimized in gas phase using the PBE/TZVP approach. The optimization procedure was then divided into two stages: first, the core of the clusters was optimized, followed by the optimization of the ligand orientations. The lowest energy conformations including the gas phase minima were then selected for the cross-checking with PBE-D/TZVPP level of theory and for the COSMO calculations in order to compare their relative energy differences in aquatic solutions.

We first focus on the structural characteristics and solvation of the cationic $[\text{Al}_5\text{O}_6\text{H}_2\text{Cl}_4]^+$ ($m/z = 373$) aluminum (chloro)hydroxide clusters. The core of the gas phase minimum of this cluster is composed of a netlike structure of Al_5O_4 and resembles closely the minimum energy structure of $[\text{Al}_5\text{O}_4]^-$ anion introduced in the studies of Das et al.^{33,34} However, the two hydroxo bridges between the corner aluminum atoms are bending the core structure from the symmetric planar configuration to a asymmetric form, see structure (a) in Figure 1. The minimum energy structure seems to be a combination of a trimeric ($[\text{Al}_3\text{O}_3(\text{OH})\text{Cl}_2]^0$) with C_{3v} symmetry and dimeric ($[\text{Al}_2\text{O}(\text{OH})\text{Cl}_2]^+$) aluminum complexes, which both have cores resembling closely to the dimeric and trimeric aluminum (chloro)hydroxides introduced in our previous studies.^{41,66} However, these substructures were not seen individually in the ESI MS studies of Sarpola et al.^{13–16}

The structure (a) consists of four equivalent three coordinated oxygen atoms and two hydroxo bridges. The core aluminum–oxygen ($R_{\text{Al}-\text{O}}$) bond distances varied from 1.79

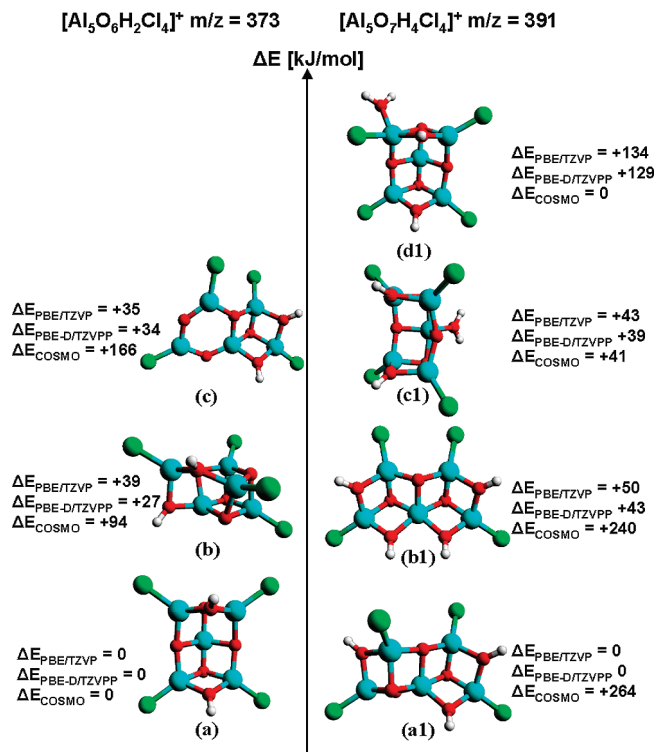


Figure 1. Optimized low energy configurations for the cationic $[Al_5O_6H_2Cl_4]^+$ and $[Al_5O_7H_4Cl_4]^+$ aluminum complexes. The energy differences are calculated relative to the gas phase and COSMO minima. Aluminum is presented in blue, oxygen in red, chlorine in green, and hydrogen in white.

to 1.89 Å, being the shortest between the center aluminum atom and trivalent oxygen bridges located between corner aluminum atoms. The corner aluminum and hydroxo bridge oxygen atom (R_{Al-OH}) bond lengths were around 1.86 Å, whereas the corner aluminum atom and trivalent core oxygen atom bond distances varied from 1.83 Å to 1.89 Å, indicating the asymmetry of the structure. All aluminum–oxygen bond lengths mentioned above differed slightly from the equivalent bond distances in the $[Al_5O_4]^-$ anion of Das et al.^{33,34} This is mainly due to the strongly electronegative chlorido ligands attached to all four corner aluminum atoms. The chlorido ligands attract valence electrons from the aluminum atoms, thereby weakening other bonds of the cluster. The aluminum–chlorine (R_{Al-Cl}) bond lengths were around 2.07 Å. Despite this ligand effect, all aluminum–oxygen (R_{Al-O}) bond lengths were within the typical Al–O single bond distance range.^{67,68}

According to the previous studies, aluminum prefers octahedral coordination in aquatic environments.^{27,28,69} However, also 5-fold coordination has been detected for the aluminum ions in solutions.^{66,70} In the case of cationic $[Al_5O_6H_2Cl_4]^+$ minimum, all five aluminum atoms in the structure were four coordinated, indicating that the complex is an ideal Lewis acid for accepting an electron pair from surrounding aqua ligands in the aquatic environments. In other words, it has a vacant coordination position in the valence shell making it ideal for acting as an acceptor of a new donor aqua ligand. Due to these hypotheses, the gas phase minima of this oligomeric aluminum complex was chosen for the CPMD simulations.

The structure (b) was chosen here not only due to its low energy but also because it has a core structure that resembles closely to the core of an intermediate tetrameric aluminum chlorohydrate $[Al_4O_2(OH)_3Cl_4]^+$ form between adamantane-like and cubane-like structures.⁴¹ The aluminum–oxygen (R_{Al-O}) bond lengths varied from 1.78 to 1.89 Å, and the R_{Al-Cl} bonds varied from 2.05 to 2.08 Å, respectively. The structure had also four equivalent trivalent oxygen atoms bridging simultaneously three different aluminum atoms leading to a tetrahedral coordination of the aluminum atoms. Structure (b) was also selected for the CPMD investigations in order to investigate its stability in aquatic environments.

The structure (c) can be considered as a combination of neutral dimeric $[Al_2O_2Cl_2]^0$ and cationic trimeric $[Al_3O_2(OH)_2Cl_2]^+$ (C_{3v} symmetry) aluminum complexes, as seen in Figure 1. The core structure has a hexagon part and a compact trimeric part sharing one aluminum and one oxygen atom. It consists of two trivalent oxygen, two bivalent oxygen atoms, and two hydroxo bridges. The aluminum–oxygen bond distances varied from 1.69 to 1.88 Å, being the shortest on the aluminum and oxygen atoms in the hexagon. The aluminum–chlorine bond distances were around 2.07 Å. Structure (c) differs from the rest of the conformations by having two three coordinated aluminum atoms in the hexagon side. However, all three aluminum atoms in the trimeric side preferred 4-fold coordination. The structure (c) was also selected for the CPMD simulations. The results of the simulations will be discussed more closely in the following sections.

The stability of the gas phase optimized structures was then investigated in aquatic environments with COSMO. Results showed clearly that the gas phase minimum of the cationic $[Al_5O_6H_2Cl_4]^+$ cluster was solvated most effectively having the lowest solvation energy. The structure (b) had around 94 kJ mol⁻¹ and the structure (c) had around 166 kJ mol⁻¹ higher solvation energies compared to the structure (a).

The minimum energy structure of the cationic $[Al_5O_7H_4Cl_4]^+$ complex consists of two trimeric parts facing in the opposite direction; see structure (a1) in Figure 1. The trimeric part on the left-hand side is facing away from the viewer, and the trimeric part on the right-hand side is facing toward the viewer, respectively. The orientation seems to be crucial, since the conformation where both trimeric parts are facing in the same direction is over 40 kJ mol⁻¹ higher in energy (PBE-D/TZVPP). The structure of the complex consists of three equivalent three coordinated oxygen atoms and four hydroxo bridges. The aluminum–oxygen bond lengths varied from 1.81 to 1.92 Å, being the longest between center five coordinated aluminum atom and top trivalent oxygen atom, which is linking the two trimeric parts together. The R_{Al-OH} bond lengths varied from 1.86 to 1.88 Å. The structure consists of four chlorido ligands attached to the corner aluminum atoms. The aluminum chlorine bond distances were around 2.08 Å. All aluminum atoms were four coordinated except the shielded center aluminum atom, which had 5-fold coordination. The core structure of the gas phase minimum was also slightly bent, which can be seen from

the 130° angle between the oxygen atom of the hydroxo bridge, center five coordinated aluminum atom, and the oxygen atom of the bridging hydroxo group of the other trimeric part.

As a gas phase minimum, the structure (**a1**) was also selected for the CPMD simulations. The selection was based also on the geometrical characteristics of the cluster because the compact trimeric unit is also one of the main components of the tridecameric Keggin cation, which can be viewed as four trimeric $\text{Al}_3\text{O}(\text{OH})_6(\text{H}_2\text{O})_3$ groups linked together at polyhedral edges around the central $\text{Al}(\text{O})_4$ unit.^{71–74} Furthermore, Keggin cation is widely considered to be one of the main hydrolysis products of aluminum in acidic aquatic solutions.^{13–17,28} Thus, the investigation of the stability of the structure (**a1**) in aquatic environments is justified.

The structure (**b1**) differs from the gas phase minimum by the orientation of the trimeric units. In (**b1**), they are both facing toward the viewer, see Figure 1. Furthermore, the two four-rings in both sides of the center five coordinated aluminum atom are in the same horizontal plane. The structure consists of four hydroxo bridges and three trivalent oxygen bridges. The $R_{\text{Al}-\text{O}}$ and $R_{\text{Al}-\text{Cl}}$ bond lengths were very similar compared to the equivalent bond distances in the structure (**a1**). The $R_{\text{Al}-\text{O}}$ bond lengths varied from 1.81 to 1.93 Å. The core of the structure (**c1**) is identical to the structure (**a**), although an additional aqua ligand is attached to the center aluminum atom increasing the coordination of aluminum from four to five. The $R_{\text{Al}-\text{OH}_2}$ bond length was 1.90 Å. In the structure (**d1**), the aqua ligand is attached to the apical position of the left aluminum atom at a distance of 1.93 Å. In this position, the aqua ligand changed also the orientation of the chlorido ligand attached to the same aluminum atom. This can be detected by comparing the bond angles between chloride, corner aluminum, and center trivalent oxygen atoms. The normal angle is around 123.0° ; however, due to the aqua ligand, this angle decreased to 107.6° , changing also the bonding of the aluminum atom from tetrahedral to trigonal-bipyramidal.

The solvation of the gas phase optimized structures with COSMO changed the energy differences of the reported structural isomers. According to the results, the two most effectively solvated structures were (**c1**) and (**d1**), as seen in Figure 1. Cavity model results indicated also that the additional water molecule is most likely attached as aqua ligand to the primary hydration shell of structure (**a**) without changing the core. Furthermore, COSMO calculations revealed that the hydration reaction from the structure (**a**) to structure (**d1**) is strongly exothermic. The Gibbs free energy of hydration (ΔG_{hyd}) was under -40 kJ mol^{-1} . This shows unambiguously that the structure (**a**) is most likely spontaneously hydrated in aqueous environments.

The search of the ground state structure of the oligomeric $[\text{Al}_5\text{O}_8\text{H}_6\text{Cl}_4]^+$ complex was demanding. Not only the amount of structural isomers in the energy surface increased compared to the previous clusters but also three different pentameric aluminum conformations within 2 kJ mol^{-1} (PBE-D/TZVPP) to the ground state structure were detected; see structures (**a2**), (**b2**), and (**c2**) in Figure 2. The common structural characteristic of these conformations was that they

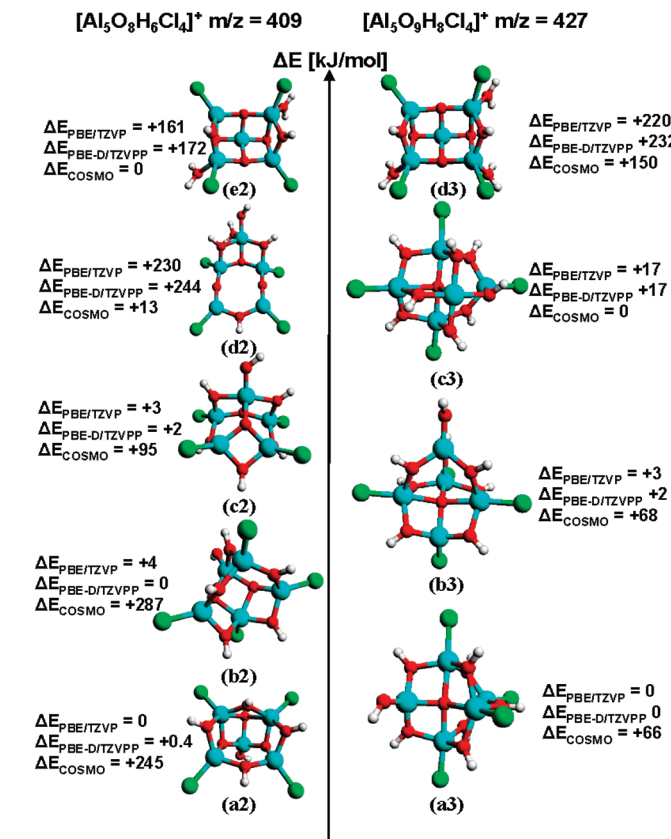


Figure 2. Optimized structures for the cationic $[\text{Al}_5\text{O}_8\text{H}_6\text{Cl}_4]^+$ and $[\text{Al}_5\text{O}_9\text{H}_8\text{Cl}_4]^+$ aluminum complexes.

all were consisted of four- and six-rings. In addition, the coordination of aluminum varied from four to five.

The core of the (**a2**) structure consists of a chain of four-rings linked together to a hexagonal shaped ring from both ends with a single hydroxo bridge; see Figure 2. From three to five aluminum atoms were four coordinated, the rest having 5-fold coordination. The two apical aluminum atoms were also joined together with a hydroxo bridge. Structurally, the most interesting detail is the protonated oxygen atom between the two apical aluminum atoms, located behind the hydroxo bridge. It is joining three different aluminum atoms together while being protonated. The $R_{\text{Al}-\text{O}}$ bond distances varied from 1.68 to 2.14 Å, being the shortest between the center aluminum and oxygen atom of hydroxo ligand. The longest aluminum–oxygen distances were between four coordinated protonated oxygen atoms and the two apical aluminum atoms. The rest of the aluminum–oxygen bond distances varied from 1.79 to 1.94 Å, and $R_{\text{Al}-\text{Cl}}$ bond lengths varied from 2.08 to 2.09 Å.

The structure (**b2**) can be considered as a combination of tetrameric $[\text{Al}_4\text{O}_2(\text{OH})_3\text{Cl}_3]^{2+}$ and monomeric $[\text{Al}(\text{OH})_3\text{Cl}]^-$ linked together through hydroxo bridges. The tetrameric part consists of three four-rings of $\text{Al}-\text{O}$ or $\text{Al}-\text{OH}$ sides. The monomeric part is then bridging three corner aluminum atoms of the tetrameric part. The core $R_{\text{Al}-\text{O}}$ bond lengths varied from 1.77 to 1.95 Å. The $R_{\text{Al}-\text{OH}_{\text{ligand}}}$ bond distance was around 1.68 Å, whereas $R_{\text{Al}-\text{Cl}}$ bond lengths varied from 2.08 to 2.10 Å.

Structure (**c2**) consists of two six-rings sharing one $\text{Al}-\text{O}$ side and linked together with one hydroxo and one trivalent

oxygen bridge; see Figure 2. It consists of four equivalent aluminum atoms with 4-fold coordination and one aluminum atom with 5-fold coordination. The core $R_{\text{Al}-\text{O}}$ bond lengths varied from 1.76 to 1.98 Å whereas the $R_{\text{Al}-\text{Cl}}$ bond distances were around 2.8 Å. The $R_{\text{Al}-\text{OHligand}}$ bond distance was around 1.71 Å. Compared to the other two structures close in energy, (**c2**) was most open. Although the structure (**b2**) was slightly lower in energy compared to the other two structures, one cannot say which one of these conformations is the real gas phase minimum. The energy difference of these structures was investigated also with second-order Møller–Plesset perturbation theory with triple ζ valence with double polarization basis set (TZVPP).^{36,42–44} However, all three conformational isomers remained within 5 kJ mol⁻¹.

The core structure (**d2**) consists of a trimeric part $[\text{Al}_3\text{O}(\text{OH})_3(\text{H}_2\text{O})\text{Cl}_2]^{2+}$ linked together with a dimeric part $[\text{Al}_2\text{O}_2(\text{OH})\text{Cl}_2]^-$ via divalent oxygen bridges. The structure consists of two four-rings and one eight-ring. The $R_{\text{Al}-\text{O}}$ bond lengths varied from 1.65 to 1.95 Å, whereas $R_{\text{Al}-\text{Cl}}$ distances varied from 2.07 to 2.13 Å. The shortest (1.65 Å) aluminum–oxygen bond lengths were between aluminum atoms of the dimeric part and divalent oxygen bridges. The core of (**d2**) resembles closely to the core of (**c2**) but is even more open. The core of (**e2**) is almost identical with the core of (**a**). The only difference is the orientation of the two chloride ligands caused by the addition of two aqua ligands to the corner aluminum atoms in the opposite sides of the structure. Due to these ligands, the bond angles between chloride, corner aluminum, and center trivalent oxygen atoms decreased to 108°. In the case of four coordinated aluminum atoms, the equivalent bond angle stayed in 121°. The $R_{\text{Al}-\text{OH}_2}$ bond lengths were around 1.93 Å.

The solvation of the gas phase optimized structures showed that the structure (**c2**) was lower in energy in aquatic solutions compared to the more compact structures (**a2**) and (**b2**); see Figure 2. In addition, the structure (**e2**) was detected to be the liquid phase minimum, although the (**d2**) seemed to be the best solvated structure overall. This is clearly due to the more exposed core structure of (**d2**). According to the COSMO calculations, the hydration reaction from (**d1**) to (**e2**) was exothermic ($\Delta G_{\text{hyd}} = -40$ kJ mol⁻¹). This indicated that the structure (**a**) experiences most likely at least two spontaneous hydration reactions in aquatic environments. The Gibbs free energy of the hydration of (**d1**) to (**d2**) was also negative ($\Delta G_{\text{hyd}} = -27$ kJ mol⁻¹), indicating that the core of the structure (**a**) can also open up in aquatic solutions.

The structural isomers of oligomeric $[\text{Al}_5\text{O}_9\text{H}_8\text{Cl}_4]^+$, especially the structure (**a3**), (**b3**), and (**c3**) had almost identical adamantane-like cores. The differences in energy were due to the different ligand orientations. The structures (**a3**) and (**c3**) were basically combinations of tetrameric $[\text{Al}_4\text{O}(\text{OH})_5\text{Cl}_2]^{2+}$ and monomeric $[\text{Al}(\text{OH})_3\text{Cl}]^-$ aluminum species. Their only difference was the additional hydroxo bridge between center aluminum atoms in the tetrameric part of the structure (**c3**). The structure (**a3**) was lacking this bridging agent, and the hydroxo group was attached as a ligand to the center aluminum atom in the left side of the tetrameric part; see Figure 2. This change in the orientation

affects to the total energy of the cluster over 15 kJ mol⁻¹. The structure of the tetrameric part closely resembled the highly compact cyclic structures of the largest stable configurations of cationic $[\text{Al}_4\text{O}(\text{OH})_5\text{Cl}_4(\text{H}_2\text{O})_{0-2}]^+$.⁴¹ The $R_{\text{Al}-\text{O}}$ bond lengths varied from 1.81 to 2.15 Å, whereas $R_{\text{Al}-\text{Cl}}$ bond distances varied from 2.09 to 2.13 Å.

The core of the structure (**b3**) can be considered as a combination of the tetrameric $[\text{Al}_4\text{O}(\text{OH})_4\text{Cl}_4]^{2+}$ and monomeric $[\text{Al}(\text{OH}_4)]^-$ units. The only difference between the structures (**a3**) and (**b3**) was the location of the hydroxo ligand. In structure (**b3**), the hydroxo ligand is attached to the aluminum atom of the monomeric part, whereas in (**a3**) it is attached to the center aluminum in the left side of the tetrameric part, as seen in Figure 2. This, however, affects very mildly the relative energy differences of the structural isomers. The $R_{\text{Al}-\text{O}}$ bond distances of the (**b3**) varied from 1.81 to 2.06 Å, and $R_{\text{Al}-\text{Cl}}$ bond lengths varied from 2.08 to 2.14 Å. Every one of the aforementioned structures ((**a3**), (**b3**), and (**c3**)) consists of three aluminum atoms with 5-fold coordination and two aluminum atoms with 4-fold coordination.

The structure (**d3**) had the same core as the structure (**a**) having three aqua ligands attached to the corner aluminum atoms. The bond angles between chloride, corner aluminum, and center trivalent oxygen atoms were approximately 108° for aluminum atoms with 5-fold coordination and 123° for aluminum atoms with 4-fold coordination. The $R_{\text{Al}-\text{OH}_2}$ bond lengths varied from 1.94 to 1.95 Å. Note that all aqua ligands were oriented to the back of the structure.

COSMO calculations changed the ground state conformation from the gas phase minimum (**a3**) to (**c3**). In total, the structure (**c3**) had over 80 kJ mol⁻¹ lower solvation energy compared to the gas phase minimum. The Gibbs free energy of hydration from (**e2**) to (**c3**) was strongly exothermic ($\Delta G_{\text{hyd}} < -200$ kJ mol⁻¹). On the grounds of these COSMO calculations, it is clear that the low coordinated pentameric aluminum clusters are most probably spontaneously hydrated in aquatic solutions. Furthermore, there is a high probability that the core structure of the pentameric complexes changes from compact to more open in liquid conditions. Thus, one of the main goals of the proceeding CPMD part is to investigate the hydrolysis and stability of the aforementioned oligomeric aluminum complexes in aquatic environments.

3.2. Car–Parrinello Molecular Dynamics Studies. In this part, we will concentrate on both the stability of the chosen pentameric aluminum complexes and their hydrolysis reactions in aquatic environments. We note that none of the previous computational studies have focused on the stability and solvation of this kind of oligomeric aluminum compounds. Thus, on the grounds of the results, we are able to improve the prevailing conception of the role of pentameric aluminum clusters in the hydrolysis of aluminum species.

3.2.1. $[\text{Al}_5\text{O}_6\text{H}_2\text{Cl}_4]^+$ (*a*) without vdW Corrections. The initial system contained 141 explicit water molecules around the cluster (**a**) in a cubic box with 17 Å sides. The total duration of the simulation was 40 ps (ps). During this time, we detected significant changes in the primary hydration shell of the cluster. In addition, due to these spontaneous reactions, the core structure of the pentameric aluminum cluster

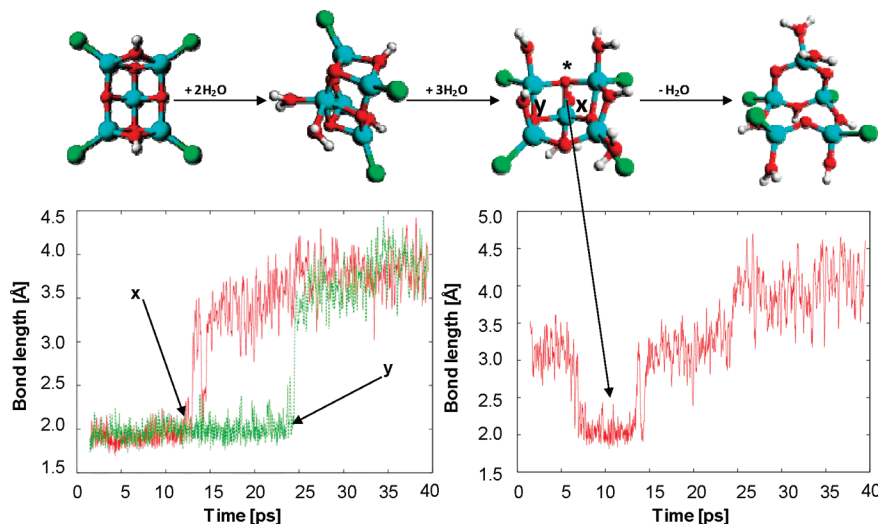


Figure 3. Detected spontaneous associative and dissociative hydration reactions in the simulation of pentameric aluminum complex (**a**). The oscillation of the Al–O bond distances (**x** and **y**) (lower left) and the oscillation of the $\text{Al}_{\text{center}}\text{--O}^*$ bond (lower right) indicating the metastability of the hexagonal prism-like structure.

changed from a compact cyclic form to an open structure; see Figure 3.

The first two aqua ligands were attached to the center aluminum atom of the ground state structure (**a**). Due to these associative hydration reactions, two of the intramolecular bonds between center aluminum and trivalent oxygen atoms on the left and right side of the core of cluster (**a**) were broken; see Figure 3. Bond dissociation was then followed by three associative hydration reactions to the corner aluminum atoms of the structure. We note that all of these hydration reactions occurred during the first 7 ps. During these reactions, the coordination of aluminum increased from four to five. However, one of the corner aluminum atoms was not hydrated, maintaining a 4-fold coordination. The lifetime of this highly symmetric and coordinated intermediate structure was from 7 to 8 ps; see the valley in the lower right corner in Figure 3. In addition, the core of this intermediate structure closely resembled the core of (**a2**). Before the addition reaction of a new aqua ligand to the open coordination position of the four coordinated aluminum atom, the dissociation of one of the already attached aqua ligands occurred (12 ps), leading to an opening of the structure.

The mechanism for the structural reorganization was as follows; first, the Al–O bonds between the center aluminum and trivalent oxygen atom (between bonds **x** and **y**) and **x** were broken, following the breakage of the bond **y** around 23 ps; see Figure 3. The newly formed structure consisted of one six- and one eight-rings, as seen from the final structure in Figure 3. During these reactions, the coordination of aluminum decreased back to four. The final open structure stayed intact for the last 15 ps without any hydration reactions. The opening of the structure indicated clearly that the gas phase ground state structure was unstable in aquatic solutions, which agrees well with the earlier COSMO findings.

3.2.2. $[\text{Al}_5\text{O}_6\text{H}_2\text{Cl}_4]^+$ (a**) with Empirical vdW Corrections.** The effect of the van der Waals corrections was investigated by employing empirical parameters to describe the vdW interactions within DFT-PBE. The starting geometry of the system

was identical compared to the previous simulation. The total duration of the simulation was around 30 ps. During the simulation, six spontaneous associative hydration reactions occurred. The mechanism for the reactions was as follows; the first two water molecules were attached to the center aluminum atom raising its coordination temporarily from four to six; second, two of the corner aluminum atoms were successively hydrated raising the coordination of aluminum from four to five; see Figure 4. The fifth additional water molecule was attached to the same corner aluminum atom as the fourth aqua ligand (circulated in the middle structure in Figure 4.) raising its coordination temporarily from five to six. Finally, the sixth aqua ligand was attached to the same aluminum atom as the third aqua ligand leading to a 6-fold coordination of aluminum. During these reactions, the structure experienced also two intramolecular aluminum–oxygen bond breakings leading to an opening of the structure.

The mechanism of the spontaneous hydration reactions occurred with similar mechanism compared to the same simulation without empirical vdW corrections. The first four hydration reactions followed the same path with only one exception: the fourth aqua ligand (circulated in the third structure in Figure 4) was attached to the equatorial position herein, whereas it was attached to the axial position in the previous simulation. In addition, the first two intramolecular Al–O bond breakings followed an identical path compared to the previous simulation. The most significant difference between the simulations mentioned above was that the third intramolecular Al–O bond **y** was broken in the simulation without empirical corrections whereas it stayed intact during the vdW-corrected simulation, preventing the structure to fully open. During this simulation, spontaneous dissociation of one of the chloride ligands was also observed. After the breakage of the aluminum-chloride bond, the newly formed chloride ion diffused and solvated around 5 Å off the cluster, decreasing the coordination of aluminum to five. The detected dissociation reaction is consistent with the Al–Cl bond dissociation energy barriers determined in our previous computational studies.⁶⁷

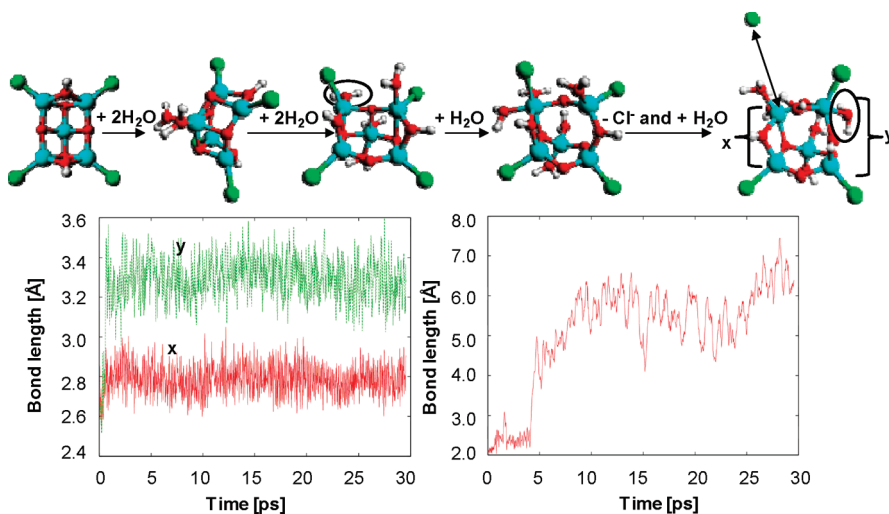


Figure 4. Detected spontaneous associative hydration reactions and the dissociation of the chloride ion. The oscillation of the Al–Al distances (lower left) of the corner aluminum atoms in the eight-ring of the cage-like structure in the vdw-corrected simulation indicating the stability of the cluster and the Al–Cl bond oscillation and the bond breaking in the lower right corner.

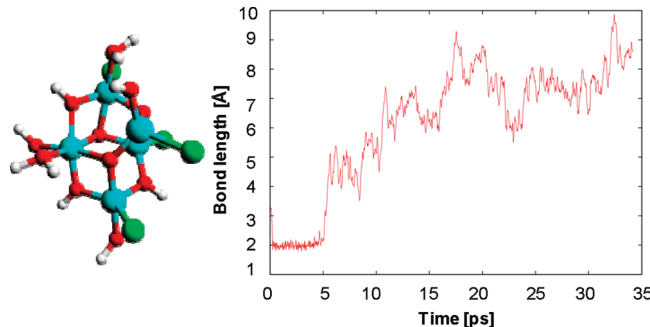


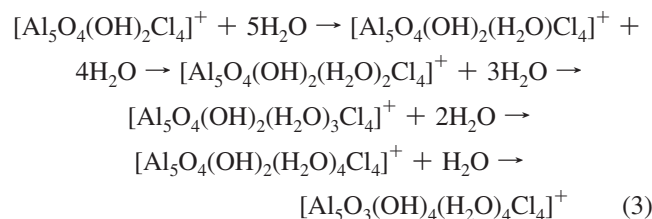
Figure 5. Final geometry in the simulation of the pentameric complex (**b**) (left) and the oscillation of the Al–O bond distance pointing the dissociation of one of the aqua ligands from the primary hydration shell (right).

We note that the first five hydration reactions and the dissociation of the chlorido ligand occurred during the first 5 ps of the simulation, indicating faster reaction speeds compared to the previous simulation. The hydration seemed to proceed further even with shorter simulation times. This agrees well with the results of the liquid water investigation of Lin et al.⁷⁵ They postulated that the vdw-corrected DFT-BLYP produces improved structural and dynamical properties of the liquid water increasing the self-diffusion coefficient and making the water softer and more liquid-like.⁷⁵ The final sixth additional aqua ligand in the equatorial position (circled in Figure 4) was attached to the primary hydration shell of the cage-like complex around 28 ps of the simulation.

The final cage-like structure consists of one four-, one six-, and one eight-ring; see Figure 4. It closely resembles the intermediate structure after the first two internal aluminum–oxygen bond breakages in the previous simulation. The oscillation (no visible drift) of the corner Al–Al distances of the eight-ring revealed that, although the structure was asymmetric, it remained intact during the last 25 ps of the simulation. The core remained intact also after the final sixth spontaneous hydration reaction. The structural reorganization and the opening of the cluster strengthened our previous

conclusions that the original structure is not stable in aquatic environments. The final sum molecular formulas of the simulations of the ground state structure (**a**) were $[Al_5O_4(OH)_3(H_2O)_5Cl_3]^+$ with and $[Al_5O_3(OH)_4(H_2O)_3Cl_4]^+$ without vdw corrections.

3.2.3. $[Al_5O_6H_2Cl_4]^+$ (b**) without vdw Corrections.** The structure (**b**) was also surrounded by 141 water molecules to a cubic cell of 17 Å sides. The total duration of the simulation was around 33 ps, in which the core of the gas phase optimized structure experienced six spontaneous hydration reactions. We note that all of these associative hydration reactions occurred in the first 4 ps of the simulation. In addition, one of the aqua ligands dissociated from the primary hydration shell back to the solution around 5 ps; see Figure 5. The sum reaction mechanism for the hydration reactions was as follows



The first two aqua ligands were attached to the aluminum atom without chlorido ligand, increasing the coordination of aluminum from four to six; see structure (**b**) in Figure 1. This was followed by the hydration of the two top corner aluminum atoms of the cubane-like moiety. During these reactions, the coordination of the corner aluminum atoms raised from four to five. After the fourth spontaneous associative hydration reaction, the intramolecular Al–O bond between the aforementioned six coordinated aluminum and trivalent oxygen atom was broken, slightly opening the structure and decreasing the coordination of aluminum from six to five. This was then followed by the hydration of the remaining four coordinated aluminum atoms. After the associative hydration reactions, the fourth additional aqua

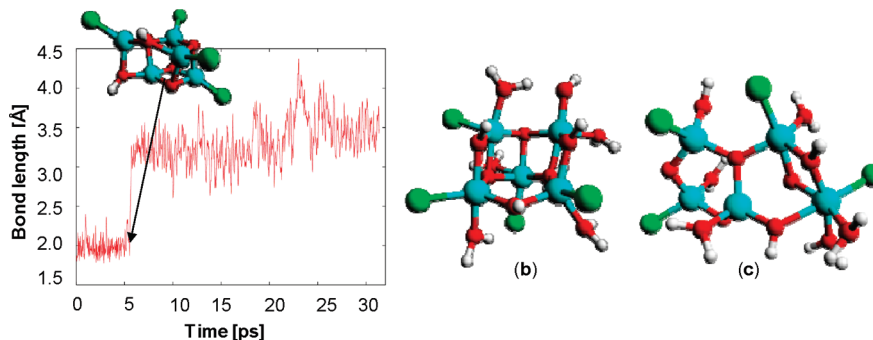


Figure 6. Al–O bond (arrow) oscillation indicating the opening of the structure (**b**) in vdW-corrected simulation (left), the final structure of (**b**) in vdW-corrected simulation (middle), and the final structure of (**c**) in the vdW-corrected simulation (right).

ligand dissociated off from the cluster; see Figure 5. During this simulation, one of the aqua ligands was also deprotonated. The dissociated proton was then captured by one of the core oxygen atoms. This intramolecular proton transfer led to a formation of bridging hydroxyl group and additional hydroxo ligand; see the final formula in eq 3.

The final structure after the last step of the simulation consisted of three equivalent oxygen bridges with 3-fold coordination and three hydroxyl bridges. Furthermore, the coordination of aluminum varied from four to six. Besides the hydration reactions, the structure (**b**) experienced only minor structural changes during the simulation. The sum molecular formula of the final structure was $[Al_5O_3(OH)_4(H_2O)_4Cl_4]^+$, as seen in Figure 5.

3.2.4. $[Al_5O_6H_2Cl_4]^+$ (b**) and (**c**) with Empirical vdW Corrections.** The simulation was performed as before and the total duration was around 32 ps. During this time, the cluster experienced seven spontaneous hydration reactions. The first six associative hydration reactions occurred during the first 5 ps, and the last seventh aqua ligand was attached to the primary hydration shell of the cluster around 21 ps. The mechanism for the reactions went as follows; first, two aqua ligands were attached to the aluminum atom without chlorido ligand, followed by three successive hydration reactions of the four coordinated aluminum atoms. The sixth additional aqua ligand, however, was attached to the corner aluminum atom of the cubane-like moiety with 5-fold coordination. Finally, the seventh associative hydration reaction occurred in the only remaining four coordinated aluminum atoms; see Figure 6.

During the simulation, the core of the complex (**b**) experienced significant topological changes, triggered by the breaking of the intramolecular Al–O bond (arrow in Figure 6) around 6 ps. The bond was broken between the center aluminum atom without chlorido ligand and the trivalent oxygen bridge facing toward the viewer; see Figure 1. The newly formed structure consisted of a chain of four Al_2O_2 -rings linked together to a hexagonal shaped ring from both ends of the chain with a single hydroxo bridge. The core of this highly symmetric structure closely resembled the core of the gas phase optimized (**a2**) and was almost identical with the core of the metastable (~ 8 ps) intermediate structure in the simulation of the structure (**a**) without empirical corrections; see Figures 2 and 4. In the case of the newly formed hexagonal prism-like structure, however, the structure stayed intact during the rest of the 25 ps of the simulation,

indicating the stability of the structure in aquatic environments; see Figure 6. This is due to the different ligand orientation compared to the metastable structure in the simulation of the structure (**a**).

The most noticeable differences were the following: first, the center aluminum atom in the structure is six coordinated whereas in the metastable structure it was five coordinated; second, one of the chlorido ligands is attached to the center aluminum atom while chlorido ligands were attached only to the corner aluminum atoms in the intermediate structure. The differences in the stability can then be explained by decreased ligand repulsion and structural straining in the complex. The final structure ((**b**) in Figure 6) closely resembles also the hexagonal prism-like crystal structure of Harlan et al.⁷⁶ However, their crystal structure analogue contained six aluminum atoms instead of five.⁷⁶ The final sum molecular formula of the newly formed pentameric aluminum complex can be written as $[Al_5O_3(OH)_4(H_2O)_6Cl_4]^+$, indicating further hydrolysis compared to the identical simulation without empirical vdW corrections.

The stability of the structure (**c**) was investigated only in a simulation of 141 explicit water molecules with empirical van der Waals corrections. The structure experienced six spontaneous associative hydration reactions during the 41 ps production run. The only topological change of the cluster during the simulation besides aforementioned hydration reactions was the opening of the Al–O bond between center aluminum atom and the trivalent oxygen bridge of the trimeric moiety. This was caused by intramolecular proton diffusion from one of the aqua ligands in the primary hydration shell to the trivalent oxygen atom. Otherwise, the core of the structure remained intact during the simulation, indicating that the structure is rather stable in liquid conditions; see Figure 6. The final sum molecular formula of the cluster can be written as $[Al_5O_3(OH)_4(H_2O)_5Cl_4]^+$.

3.2.5. $[Al_5O_7H_4Cl_4]^+$ (a1**) without vdW Corrections.** The initial system contained 169 explicit water molecules around the cluster (**a1**) in a cubic box with 18 Å sides. The total duration of the simulation was around 44 ps. During this time, the topology of the cluster changed significantly from highly symmetric cyclic to an open structure. A pentameric aluminum complex (**a1**) experienced in a total of four associative hydration reactions. In addition, the breaking of the intramolecular Al–O bond between the center aluminum atom and the topmost trivalent bridging oxygen atom occurred; see Figure 1. The final structure of the simulation

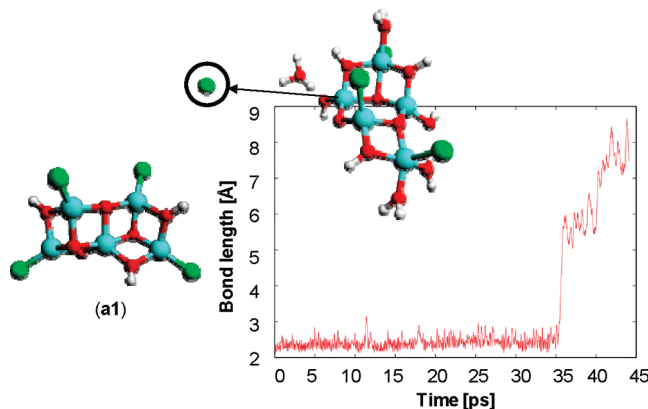


Figure 7. Initial gas phase structure (left), the Al–Cl bond oscillation indicating the dissociation of the chlorido ligand, and the final geometry of the simulation (right).

can be considered as a combination of adamantane-like tetrameric moiety $[Al_4O_3(OH)_3(H_2O)_2Cl_2]^+$ and a monomeric moiety $[Al(OH)(H_2O)_2Cl]^+$; see Figure 7. We note that the four hydration reactions and the intramolecular bond breakage occurred during the first 9 ps.

During the simulation (~ 35 ps), the dissociation of one of the chlorido ligands was also observed; see Figure 7. After the breakage of the aluminum–chlorine bond, the newly formed chloride ion (circulated) was diffused further and solvated 6 to 8 Å off the cluster, decreasing the coordination of aluminum from five to four. The breaking of one of the intramolecular Al–O bonds between the center aluminum atom and oxygen atom of the bridging hydroxo group in the left trimeric moiety was also detected, leading to a formation of an additional hydroxo ligand. Akitt et al. suggested that this kind of hydroxo ligand formation can trigger the polymerization of monomeric aluminum species to dimeric complexes.³ In the case of monomeric species, the formation of the hydroxo ligand is due to proton transfer, but in the case of oligomeric aluminum complexes, such as (a1), the formation can be caused also by intramolecular topological changes. Detected associative hydration reactions and changes in the core structure indicated clearly that the original structure was unstable in aquatic environments. In addition, the formation of hydroxo ligand strengthened the conclusion, indicating that the structure is a likely candidate for further polymerization reactions. The final sum molecular formula of the cluster can then be written as $[Al_5O_3(OH)_4(H_2O)_4-Cl_3]^{2+}$. The charge was due to the dissociation of the chlorido ligand.

3.2.6. $[Al_5O_7H_4Cl_4]^+$ (a1) with Empirical vdW Corrections. The stability of (a1) was also tested in an identical vdW-corrected simulation of 32 ps. During this time, the gas phase optimized structure (a1) experienced four hydration reactions and three intramolecular bond breakings, leading to a significant topological changes and the opening of the ground state structure. The intramolecular Al–O bond breakings followed the same mechanism compared to the aforementioned simulation without empirical vdW corrections. The final structure of the simulation consisted of two Al–O four-rings linked together from both ends by an eight-ring, as seen in Figure 8.

Transformation of one of the bridging hydroxo groups to a hydroxo ligand was also detected, as in the previous simulation without vdW corrections. The breaking of the Al–O bond, which triggered the conversion, occurred around 16 ps of the simulation. This strengthened the previous conclusions that the structure (a1) is unstable in aquatic environments. After the structural reorganization, the newly formed open complex stayed intact experiencing only one attempt for the intramolecular Al–O bond dissociation between 16 and 23 ps of the simulation; see Figure 8. The final sum molecular formula of the cluster can be written as $[Al_5O_3(OH)_5(H_2O)_3Cl_4]^0$. The neutral charge of the complex is due to the proton transfer reactions between the cluster and surrounding water molecules.

During these seven individual simulations, we detected several (4/7) structural rearrangements of the compact symmetric structures to an open or cage-like structure. The open structure and highly symmetric hexagonal prism-like structures were found to be dominating geometries for the pentameric aluminum complexes in liquid conditions. Furthermore, several spontaneous associative hydration reactions occurred in every simulation, indicating that the structures detected in the ESI MS experiments are low coordinated.^{13–16} The same phenomenon was also detected in our previous CPMD studies of the dimeric aluminum chlorohydrates in aquatic environments.⁶⁶ An interesting observation of these simulations was that the hydrolysis proceeded further in the simulations with empirical long-range vdW corrections compared to the simulations without corrections. In addition, the hydration reactions occurred faster, enabling shorter simulation times in the vdW-corrected simulations. We note that the majority of the Al–O bond lengths detected during the CPMD part of this study were within the typical Al–O single bond distance range.^{67,68}

3.2.7. Solvation of the Clusters. In this section, we concentrate on the structural characteristics of the surrounding water. This was done by investigating the total HO– and OO– radial distribution functions from the cationic $[Al_5O_7H_4Cl_4]^+$ ($m/z = 391$) system with and without empirical van der Waals corrections. The first peak in HO–RDF with the distance of 0.87–1.16 Å, maximum at 0.99 Å, corresponds to the OH distances in water molecules and in the cluster, Figure 9. The second peak at the distance of 1.29–2.40 Å gives us the total amount of acceptor and donor hydrogen bonds in the systems. The maximum of the second peak of around 1.78 Å for both systems is close to the experimental value (1.8 Å) of the hydrogen bond.^{77,78} The shapes and positions of the g(O,H) and g(O,O) RDFs in both systems are in good agreement with the water diffraction data of Soper et al.^{77,78} In OO–RDF, the first peak at the distance of 2.33–3.31, maximum at 2.73 Å, and the second peak at the distance 3.51–5.51, maximum at 4.49 Å, are almost identical to the experimental values.^{77,78} The results are also in very good agreement with the CPMD results of Sillanpää et al.²¹ and with the results of liquid water studies of Kuo et al.⁷⁹

It is known that the PBE density functional tends to slightly overstructure pair correlation functions and, in addition, the self-diffusion coefficient is much smaller than in experiments

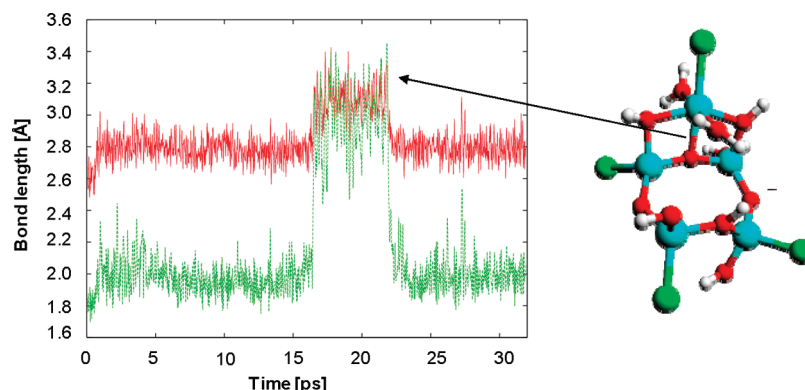


Figure 8. Oscillations of the Al–O (green) bond between the topmost aluminum atom and the center trivalent oxygen atom and Al–Al (red) distance between the topmost aluminum and the corner aluminum atom in the same four-ring are indicating the stability of the final open structure (right). The peak in the figure corresponds to the intramolecular Al–O bond breaking.

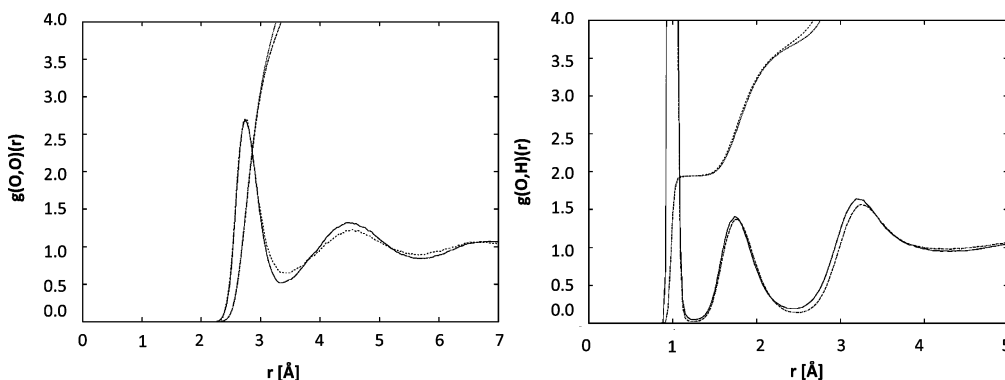


Figure 9. Differences in the total OH– and OO–RDFs of the $[Al_5O_7H_4Cl_4]^+$ ($m/z = 391$) simulation with and without empirical vdW corrections. Dashed line indicates the system with empirical corrections in $g(O,O)(r)$ and in $g(O,H)(r)$; the solid line indicates the vdW-corrected system. The upper integral belongs to the vdW-corrected system, and the lower belongs to the system without empirical corrections.

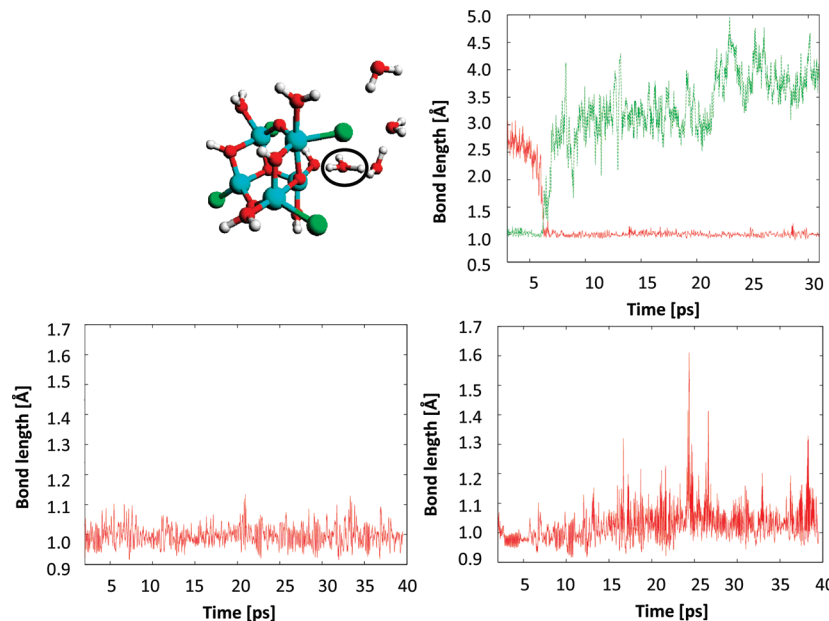


Figure 10. Oscillation of the covalent O–H bond of the aqua ligand (lower right) and the solvent water molecule (lower left). The formation of the hydronium ion (circulated) to the secondary hydration shell is in the upper left corner and the oscillation of the O–H distances indicating the intramolecular proton transfers from aqua ligand (green) to the trivalent unprotonated core oxygen atom (red) is in upper right corner.

making the water sluggish.^{80,81} However, according to the findings of Lin et al., the usage of empirical van der Waals

corrections in CPMD decreases the difference in the self-diffusion coefficient between computations and experi-

ments.⁷⁵ Although the diffusion coefficient was not measured in this study, the g(O,O) of the vdW-corrected system displayed softer structure (dashed line in Figure 9) for the water compared to the DFT-PBE simulation and closer to the experimental results of Soper et al.^{77,78} Slow diffusion should not be a problem in the systems without empirical corrections either due to the rather long simulation times and higher temperatures (350 K).⁶⁶

During the simulations, we detected several attempts of the protons of aqua ligands to jump to the surrounding water, indicating the acidity of the pentameric aluminum complexes. In the majority of the cases, the protons stayed intact in the cluster without diffusion to the surrounding solvent. In almost every simulation, however, transient proton jumps were detected. The mechanism for these proton transfers was always the same: a nearby solvent molecule captured the proton from the aqua ligand or bridging hydroxo group; see Figure 10. As a result, the hydronium ion ($[H_3O]^+$) was formed in the secondary hydration shell. This is in good agreement with the studies of Tuckerman et al.^{82,83} The acidity of the aqua ligands was also seen by observing the covalent oxygen–hydrogen bond distances. For the solvent water molecule, this distance oscillated from 0.92 to 1.1 Å with an average around 1.0 Å; whereas for the aqua ligands, the distance varied from 0.92 to 1.6 Å; see Figure 10. During these simulations, we detected also several (4/7 cases) intramolecular proton transfers from aqua ligands to the trivalent unprotonated core oxygen atoms.

4. Conclusions

We used a static quantum chemical and Car–Parrinello molecular dynamics (CPMD) approach to investigate the structural characteristics, the stability, and the hydrolysis of pentameric aluminum complexes in both gas phase and in aquatic environments. We tested the accuracy of several generalized gradient approximation (GGA) and hybrid exchange-correlation functionals in reference to the second-order Møller–Plesset perturbation theory (MP2). The PBE density functional with empirical van der Waals corrections gave the most coherent results and was selected (PBE-D/TZVPP) for the gas phase conformational analysis. In total, we analyzed hundreds of experimentally detected (ESI MS) structural isomers to find the ground state structures for cationic $[Al_5O_6H_2Cl_4]^+$, $[Al_5O_7H_4Cl_4]^+$, $[Al_5O_8H_6Cl_4]^+$, and $[Al_5O_9H_8Cl_4]^+$ complexes. The analysis revealed that the minimum energy structure was always changed when switching from one cluster to another, indicating that there is not any structural explanation for the crystallization detected in ESI MS studies of Sarpola et al.^{13–16,32}

Conductor-like screening model (COSMO) was used to investigate the stability of the gas phase optimized structures in aquatic environments. COSMO calculations revealed that the low coordinated pentameric aluminum clusters are spontaneously hydrated in aquatic solutions. Furthermore, COSMO results indicated that there is a high possibility for the gas phase ground state structures to open up in aquatic solutions, especially when the amount of aqua ligands increases in primary hydration shell. The hydration reactions

from $[Al_5O_6H_2Cl_4]^+$ to $[Al_5O_9H_8Cl_4]^+$ were also detected to be strongly exothermic ($\Delta G < 0$).

We performed seven different CPMD simulations to reveal the stability of the chosen pentameric clusters in aquatic solutions. The effect of the long-range empirical van der Waals corrections (-D) was also tested, employing two identical simulations one with and one without the corrections. During these simulations, we detected several spontaneous associative hydration reactions in the primary hydration shell, indicating that the structures detected in the ESI MS experiments are low coordinated. Hydrolysis was also detected to proceed further in vdW-corrected simulations. In addition, the hydration reactions occurred faster, enabling shorter simulation times in the DFT-PBE-D simulations.

During most of the simulations, the chosen structures experienced significant topological changes. In four out of seven cases, the compact cyclic structure was opened leading to a formation of an open or cage-like structure. The open structure, cage-like, and highly symmetric hexagonal prism-like structures were found to be dominating geometries for the pentameric aluminum complexes in liquid environments. Several spontaneous associative hydration reactions were also detected in every simulation. Although we did not find any unique structure for the clusters, the dynamics and the ability of the pentameric complexes to transform in aquatic environments was seen within the picosecond time scales of the simulations. In addition, the structural reorganization and the composition of the open structures (e.g., (a1) simulations) indicated that the Al_5 -clusters are most likely only metastable intermediate forms in the aluminum salt hydrolysis during coagulation, which is in good agreement with the ESI MS findings of Zhao et al.¹⁷

Acknowledgment. The authors thank the graduate school, LASKEMO (Academy of Finland), and the Tauno Tönnig foundation for financial support and the IT Center for Science (CSC) for computational resources and expert service. The authors also thank Professor Jürg Hutter for providing a new version of the CPMD code and Dr. Atte Sillanpää for the guidance with the code and useful discussions. Dr. Arja Sarpola is also acknowledged for general support concerning ESI MS results.

References

- (1) Brosset, C. *Acta Chem. Scand.* **1952**, 6, 910.
- (2) Van Cauwelaert, F. H.; Bosman, H. *J. Rev. Chim. Minér.* **1969**, 6 (3), 611.
- (3) Akitt, J. W.; Greenwood, N. N.; Khandelwal, B. L.; Lester, G. D. *J. Chem. Soc., Dalton Trans.: Inorg. Chem.* **1972**, 5, 604.
- (4) Bottero, J. Y.; Cases, J. M.; Fiessinger, F.; Poirier, J. E. *J. Phys. Chem.* **1980**, 84 (22), 2933.
- (5) Akitt, J. W.; Elders, J. M. *J. Chem. Soc., Dalton Trans.* **1988**, 5, 1347.
- (6) Fu, G.; Nazar, L. F.; Bain, A. D. *Chem. Mater.* **1991**, 3, 602.
- (7) Nazar, L. F.; Fu, G.; Bain, A. D. *J. Chem. Soc., Chem. Commun.* **1992**, 1992, 251.

- (8) Allouche, L.; Gérardin, C.; Loiseau, T.; Férey, G.; Taulelle, F. *Angew. Chem., Int. Ed.* **2000**, *39* (3), 511.
- (9) Allouche, L.; Taulelle, F. *Inorg. Chem. Commun.* **2003**, *6*, 1167.
- (10) Shafran, K. L.; Perry, C. C. *Dalton. Trans.* **2005**, *12*, 2089.
- (11) Johansson, G. *Acta Chem. Scand.* **1960**, *14* (3), 771.
- (12) Seichter, W.; Mögel, H.-J.; Brand, P.; Salah, D. *Eur. J. Inorg. Chem.* **1998**, *6*, 795.
- (13) Sarpola, A.; Hietapelto, V.; Jalonen, J.; Jokela, J.; Laitinen, R. S. *J. Mass Spectrom.* **2004**, *39*, 423.
- (14) Sarpola, A.; Hietapelto, V.; Jalonen, J.; Jokela, J.; Laitinen, R. S.; Rämö, J. *J. Mass Spectrom.* **2004**, *39*, 1209.
- (15) Sarpola, A. T.; Hietapelto, V. K.; Jalonen, J. E.; Jokela, J.; Rämö, J. H. *Int. J. Environ. Anal. Chem.* **2006**, *86* (13), 1007.
- (16) Sarpola, A. T.; Saukkoriipi, J. J.; Hietapelto, V. K.; Jalonen, J. E.; Jokela, J. T.; Joensuu, P. H.; Laasonen, K. E.; Rämö, J. H. *Phys. Chem. Chem. Phys.* **2007**, *9*, 377.
- (17) Zhao, Z.; Liu, H.; Qu, J. *J. Colloid Interface Sci.* **2009**, *330* (1), 105.
- (18) Gale, J. D.; Rohl, A. L.; Watling, H. R.; Parkinson, G. M. *J. Phys. Chem. B* **1998**, *102*, 10372.
- (19) Martinez, A.; Tenorio, F. J.; Ortiz, J. V. *J. Phys. Chem. A* **2001**, *105*, 8787.
- (20) Martinez, A.; Tenorio, F. J.; Ortiz, J. V. *J. Phys. Chem. A* **2001**, *105*, 11291.
- (21) Sillanpää, A. J.; Päiväranta, J. T.; Hotokka, M. J.; Rosenholm, J. B.; Laasonen, K. E. *J. Phys. Chem. A* **2001**, *105*, 10111.
- (22) Martinez, A.; Sansores, L. E.; Salcedo, R.; Tenorio, F. J.; Ortiz, J. V. *J. Phys. Chem. A* **2002**, *106*, 10630.
- (23) Martinez, A.; Tenorio, F. J.; Ortiz, J. V. *J. Phys. Chem. A* **2003**, *107*, 2589.
- (24) Bock, C. W.; Markham, G. D.; Katz, A. K.; Glusker, J. P. *Inorg. Chem.* **2003**, *42*, 1530.
- (25) Gowtham, S.; Lau, K. C.; Deshpande, M.; Pandey, R.; Gianotto, A. K.; Groenewold, G. S. *J. Phys. Chem. A* **2004**, *108*, 5081.
- (26) Ahu Akin, F.; Jarrold, C. C. *J. Chem. Phys.* **2004**, *120* (18), 8698.
- (27) Popovska, V.; Klein, M. L.; Holerca, M. N. *J. Phys. Chem. A* **2004**, *108*, 113.
- (28) Popovska, V.; Balagurusamy, V. S. K.; Klein, M. L. *Phys. Chem. Chem. Phys.* **2004**, *6*, 919.
- (29) Ikeda, T.; Hirata, M.; Kimura, T. *J. Chem. Phys.* **2006**, *124*, 074503-1.
- (30) Akitt, J. W.; Elders, J. M. *J. Chem. Soc., Dalton Trans.* **1988**, *5*, 1347.
- (31) Akitt, J. W.; Elders, J. M.; Fontaine, X. L. R.; Kundu, A. K. *J. Chem. Soc., Dalton Trans.* **1989**, *10*, 1889.
- (32) Sarpola, A. The Hydrolysis of Aluminum, A Mass Spectrometric Study. Ph.D. Dissertation, University of Oulu, Oulu, Finland, Acta Univ. Oul., 2007; C 279, pp 1–104.
- (33) Das, U.; Raghavachari, K.; Jarrold, C. C. *J. Chem. Phys.* **2005**, *122*, 014313-1.
- (34) Das, U.; Raghavachari, K. *J. Chem. Theory Comput.* **2008**, *4*, 2011.
- (35) Perdew, J. P.; Burke, K.; Ernzerhof, M. *Phys. Rev. Lett.* **1996**, *77* (18), 3865.
- (36) Schäfer, A.; Huber, C.; Ahlrichs, R. *J. Chem. Phys.* **1994**, *100* (8), 5829.
- (37) Ahlrichs, R.; Armbruster, M. K.; Bär, M.; Baron, H.-P.; Bauernschmitt, R.; Böcker, S.; Crawford, N.; Deglmann, P.; Ehrig, M.; Eichkorn, K.; Elliot, S.; Furche, F.; Haase, F.; Häser, M.; Hättig, C.; Hellweg, A.; Horn, H.; Huber, C.; Huniar, U.; Kattannek, M.; Köhn, A.; Kölmel, C.; Kollwitz, M.; May, K.; Nava, P.; Ochsenfeld, C.; Öhm, H.; Patzelt, H.; Rappoport, D.; Rubner, O.; Schäfer, U.; Sierka, M.; Treutler, O.; Utterreiner, B.; Arnim, M.; Weigend, F.; Weis, P.; Weiss, H. Turbomole Program Package for ab initio Electronic Structure Calculations, Users Manual, University of Karlsruhe and Forschungszentrum, Karlsruhe, GmbH, 1989–2007, TURBOMOLE GmbH, 2009; pp 1–341.
- (38) (a) Eichkorn, K.; Treutler, H.; Öhm, H.; Häser, M.; Ahlrichs, R. *Chem. Phys. Lett.* **1995**, *240*, 283. (b) Eichkorn, K.; Treutler, H.; Öhm, H.; Häser, M.; Ahlrichs, R. *Chem. Phys. Lett.* **1995**, *242* (6), 652.
- (39) Grimme, S. *J. Comput. Chem.* **2004**, *25* (12), 1463.
- (40) Grimme, S. *J. Comput. Chem.* **2006**, *27* (15), 1787.
- (41) Saukkoriipi, J.; Sillanpää, A.; Laasonen, K. *Phys. Chem. Chem. Phys.* **2005**, *7*, 3785.
- (42) Weigend, F.; Häser, M. *Theor. Chem. Acc.* **1997**, *97* (1–4), 331.
- (43) Weigend, F.; Häser, M.; Patzelt, H.; Ahlrichs, R. *Chem. Phys. Lett.* **1998**, *294* (1–3), 143.
- (44) Weigend, F.; Furche, F.; Ahlrichs, R. *J. Chem. Phys.* **2003**, *119* (24), 12753.
- (45) Becke, A. D. *Phys. Rev. A* **1988**, *38* (6), 3098.
- (46) Lee, C.; Yang, W.; Parr, R. G. *Phys. Rev. B* **1988**, *37* (2), 785.
- (47) Becke, A. D. *J. Chem. Phys.* **1993**, *98* (7), 5648.
- (48) Becke, A. D. *J. Chem. Phys.* **1996**, *104* (3), 1040.
- (49) Grimme, S. *J. Chem. Phys.* **2006**, *124*, 034108-1.
- (50) Schwabe, T.; Grimme, S. *Phys. Chem. Chem. Phys.* **2007**, *9*, 3397.
- (51) Schäfer, A.; Klamt, A.; Sattel, D.; Lohrenz, J. C. W.; Eckert, F. *Phys. Chem. Chem. Phys.* **1993**, *2*, 2187.
- (52) Klamt, A.; Schüürmann, G. *J. Chem. Soc., Perkin Trans. 1993*, *2*, 799.
- (53) Burgess, J. Metal Ions in Solution; John Wiley & Sons: Chichester, Sussex, England, 1978; pp 179–186.
- (54) Tissandier, M. D.; Cowen, K. A.; Feng, W. Y.; Gundlach, E.; Cohen, M. H.; Earhart, A. D.; Tuttle, T. R., Jr.; Coe, J. V. *J. Phys. Chem. A* **1998**, *102* (40), 7787.
- (55) Coskuner, O.; Jarvis, E. A. A. *J. Phys. Chem. A* **2008**, *112* (12), 2628.
- (56) Toukan, K.; Rahman, A. *Phys. Rev. B* **1985**, *31*, 2643.
- (57) Berendsen, H. J. C.; Grigera, J. R.; Straatsma, T. P. *J. Phys. Chem.* **1987**, *91*, 6269.
- (58) Parrinello, M.; Hutter, J.; Marx, D.; Focher, P.; Tuckerman, M.; Andreoni, W.; Curioni, A.; Fois, E.; Roetlisberger, U.; Giannozzi, P.; Deutsch, T.; Alavi, A.; Sebastiani, D.; Laio, A.; VandeVondele, J.; Seitsonen, A.; Billeter, S. CPMD, Car–Parrinello Molecular Dynamics. <http://www.cpmd.org/>, Copy-

- right IBM Corp 1990–2008, Copyright MPI für Festkörperforschung Stuttgart 1997–2001; pp 1–258.
- (59) Nose, S. *J. Phys. Chem.* **1984**, *81* (1), 511.
- (60) Nose, S. *Mol. Phys.* **1984**, *52* (2), 255.
- (61) Hoover, W. G. *Phys. Rev. A* **1985**, *31* (3), 1695.
- (62) Martyna, G. J. *Phys. Rev. E* **1994**, *50* (4), 3234.
- (63) Vanderbilt, D. *Phys. Rev. B* **1990**, *41* (11), 7892.
- (64) Laasonen, K.; Car, R.; Lee, C.; Vanderbilt, D. *Phys. Rev. B* **1991**, *43* (8), 6796.
- (65) Laasonen, K.; Pasquarello, A.; Car, R.; Lee, C.; Vanderbilt, D. *Phys. Rev. B* **1993**, *47* (16), 10142.
- (66) Saukkoriipi, J. J.; Laasonen, K. *J. Phys. Chem. A* **2008**, *112* (43), 10873.
- (67) Zaworotko, M. J.; Rogers, R. D.; Atwood, J. L. *Organometallics* **1982**, *1*, 1179.
- (68) Shreve, A. P.; Mulhaupt, R.; Fultz, W.; Calabrese, J.; Robbins, W.; Ittel, S. D. *Organometallics* **1988**, *7*, 409.
- (69) Fratiello, A.; Lee, R. E.; Nishida, V. M.; Schuster, R. E. *J. Chem. Phys.* **1968**, *48* (8), 3705.
- (70) Swaddle, T. W.; Rosenqvist, J.; Yu, P.; Bylaska, E.; Phillips, B. L.; Casey, W. H. *Science* **2005**, *308*, 1450.
- (71) Casey, W. H. *Chem. Rev.* **2006**, *106* (1), 1.
- (72) Johansson, G.; Lundgren, G.; Sillen, L. G.; Söderquist, R. *Acta Chem. Scand.* **1960**, *14*, 769.
- (73) Johansson, G. *Acta Chem. Scand.* **1960**, *14* (3), 771.
- (74) Keggin, J. F. *Proc. R. Soc., Ser. A* **1934**, *144*, 75.
- (75) Lin, I.-C.; Seitsonen, A. P.; Coutinho-Neto, M. D.; Tavernelli, I.; Rothlisberger, U. *J. Phys. Chem. B* **2009**, *113* (4), 1127.
- (76) Harlan, C. J.; Mason, M. R.; Barron, A. R. *Organometallics* **1994**, *13* (8), 2957.
- (77) Soper, A. K.; Bruni, F.; Ricci, M. A. *J. Chem. Phys.* **1997**, *106* (1), 247.
- (78) Soper, A. K. *J. Phys.: Condens. Matter* **2007**, *19* (33), 335206.
- (79) Kuo, I.-F. W.; Mundy, C. J.; McGrath, M. J.; Siepmann, J. I.; VandeVondele, J.; Sprik, M.; Hutter, J.; Chen, B.; Klein, M. L.; Mohamed, F.; Krack, M.; Parrinello, M. *J. Phys. Chem. B* **2004**, *108* (34), 12990.
- (80) VandeVondele, J.; Mohamed, F.; Krack, M.; Hutter, J.; Sprik, M.; Parrinello, M. *J. Chem. Phys.* **2005**, *122*, 014515-1.
- (81) Lee, H.-S.; Tuckerman, M. E. *J. Chem. Phys.* **2007**, *126*, 164501.
- (82) Tuckerman, M.; Laasonen, K.; Sprik, M.; Parrinello, M. *J. Chem. Phys.* **1995**, *103* (1), 150.
- (83) Tuckerman, M. E.; Ungar, P. J.; von Rosenvinge, T.; Klein, M. L. *J. Phys. Chem.* **1996**, *100* (31), 12878.

CT900670A